Electrified Aircraft Propulsion Controls Hardware Testing

Joseph W. Connolly*, Donald L. Simon†, Dennis E. Culley‡, Jonah Sachs-Wetstone§, Keith Hunker¶, Santino Bianco‖, and Joseph Haglage**
NASA Glenn Research Center, Cleveland, OH, 44135

Mark Bell††, Marcus Horning‡‡, Halle Buescher§§
HX5, Brookpark, OH, 44142

Electrified Aircraft Propulsion (EAP) systems hold potential for the reduction of aircraft fuel burn and emissions. To realize this potential for single-aisle aircraft, control technology challenges associated with EAP designs are increasing the demand for Hardware-In-the-Loop (HIL) studies that address the tightly coupled electrical powertrain and turbofan propulsion systems. Reconfigurable HIL testbeds enable the study of integrated supervisory control and control approaches that augment engine shaft torques to improve performance. This paper presents an overview of conceptual EAP controls architecture testing in two HIL testbeds. The NASA Electric Aircraft Testbed provides the ability for megawatt class electric powertrain testing for technology maturation. A 100 kilowatt testbed, the Hybrid Propulsion Emulation Rig, allows for rapid controls technology trade studies. In both testbeds, controls testing is performed by implementing the electrical power system in hardware while turbomachinery is emulated via electric machines that are commanded by a real-time model and controls. A novel scaling algorithm is applied to emulate the inertial loads of the turbomachinery that causes the electric machines to respond in a fashion similar to that of the full-scale propulsion system they represent. Results demonstrate desired control performance at both testbed scales for the conceptual EAP architecture.

I. Introduction

The need for aviation to reduce its environmental impact is pushing the industry to explore Electrified Aircraft Propulsion (EAP) technologies for the next generation of aircraft [1, 2]. The dominant source of emissions in the aviation market is from single-aisle aircraft [3, 4]. While there is a goal for zero emissions, for larger aircraft a hybrid design provides an intermediate step towards electrification that addresses the high energy demands and current limitations in the energy density, weight, and volume of electric energy storage devices. EAP presents both new design flexibility and new design challenges. One of the important enabling technologies for the maturation of EAP is system-level controls technology. Control systems will play a vital role in ensuring the optimal integration of electrical powertrains with turbomachinery hardware [5]. For these reasons, new approaches that introduce control technology earlier in design phase are needed.

Turbomachinery generally has a high cost-to-operate and complexities related to its operation. Implementing an untested electro-mechanical power system and its control on turbomachinery increases the financial and safety risk associated with testing. Hardware-In-the-Loop (HIL) testing is a means to bridge the gap between conceptual simulations and full-scale system hardware testing [6, 7]. To support EAP technology development, HIL facilities are being developed at the National Aeronautics and Space Administration (NASA) to support testing of electrical hardware, control algorithms, and the integration of propulsion systems with electrical powertrains. A conceptual hybrid turbofan is shown in Fig. 1a with its translation to a HIL block diagram in Fig. 1b.

*Aerospace Engineer, Research and Engineering, and AIAA Associate Fellow.
†Control Systems Engineer, Research and Engineering.
‡Control Systems Engineer, Research and Engineering, and AIAA Senior Member.
§Aerospace Engineer, Research and Engineering, and AIAA Member.
¶Electrical Engineer, Research and Engineering, and AIAA Member.
‖Control Systems Engineer, Research and Engineering.
**Electrical Engineer, Research and Engineering.
††Electrical Engineer, Research and Engineering.
‡‡Electrical Engineer, Research and Engineering.
§§Aerospace Engineer, Research and Engineering, and AIAA Senior Member.

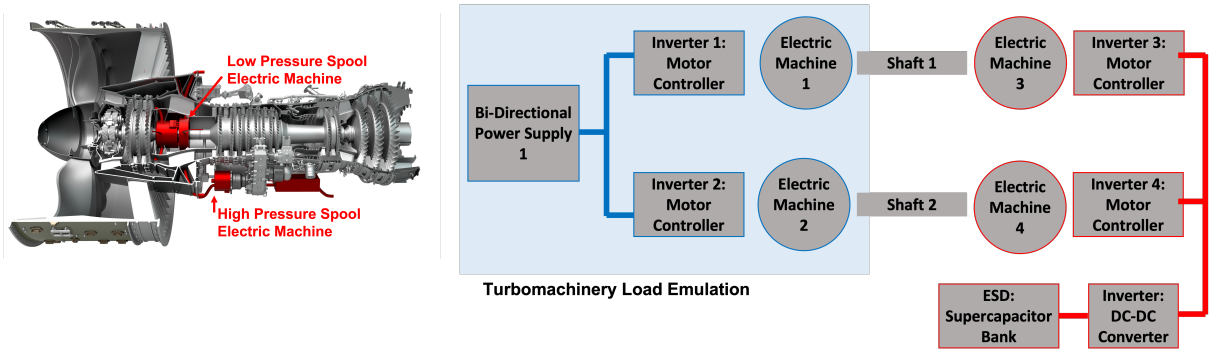

(a) Conceptual hybrid turbofan. **(b) Hardware block diagram of hybrid turbofan.**

Fig. 1 Conceptual hybrid turbofan shown in (a) is illustrated as a block diagram for the HIL implementation in (b), where blue indicates the emulated turbomachinery and red indicates the experimental electrical powertrain.

HIL testing is not new and several other HIL testbed efforts for EAP are being developed at various levels of fidelity. Smaller scale HIL facilities allow for the rapid testing of EAP concepts [8–10]; however, they typically lack the energy storage elements and do not adequately address scaling to the desired system size. Other HIL facilities have focused on the larger or full-scale testing of the electrical powertrain [11, 12]. The larger facilities offer many advantages, especially for later stage testing, but these facilities are often in high demand and thus gaining access to them is challenging. An additional key need in the EAP space is the development of facilities to address electrical standards [13, 14] while other implementations focus on controls development [15, 16]. All these approaches provide valuable capabilities needed for EAP technology maturation.

To take advantage of the various HIL testbed features a series of EAP controls tests are conducted in two NASA facilities at both a large and small scale. This enables the verification of EAP component and control algorithm operation. This paper provides an overview of those test campaigns and results that are broadly applicable to EAP HIL testing [17–20]. The NASA Electric Aircraft Testbed (NEAT) is one testbed built with the intention of testing full-scale Mega-Watt (MW) EAP powertrains at altitude [12]. The Hybrid Propulsion Emulation Rig (HyPER) is a smaller scale testbed built to test EAP control algorithms for rapid feasibility studies. In HyPER and NEAT, closed loop control and scaling are used to emulate the turbomachinery dynamic mechanical loads for each applicable engine spool or propulsor shaft. A hybrid-electric propulsion system model and its control define the desired dynamics of the EAP system and are mimicked in hardware through a closed loop control and scaling approach. This provides a low cost approach to reduce risk during initial testing of hybrid-electric propulsion architectures and control concepts. It also helps to raise the technology readiness level (TRL) of such concepts. The rest of the paper is outlined as follows. Section II provides an overview of the HIL testbeds. The real-time modeling effort is discussed in Section III for the propulsion system, controller, and dynamic scaling. Section IV provides a discussion of results spanning the recent test campaigns. Finally, some concluding remarks are made in Section V.

II. Hardware In the Loop Testbeds Overview

NEAT and HyPER are HIL testbeds used in part to investigate control technologies. They contain electro-mechanical and electrical power system components as well as closed-loop control and scaling that allows the system to dynamically represent an electrified turbomachinery shaft. The hardware components are relatively inexpensive commercial-off-the-shelf components that reduce the risk associated with the initial testing of flight or development hardware. The testbeds are structured in three parts: the emulation of a turbofan engine reproducing the mechanical shaft interface to the electrical power system, an experiment electric power system, and a dynamically variable electrical load. In order to investigate the controls concepts in these testbeds, the turbofan engine, depicted in Fig. 1, is replaced with a real-time simulation. Sets of controller/motor pairs are used to emulate the low and high pressure turbofan shafts as well as the EAP powertrain required in the control strategy to apply off-nominal torques to the shafts. The portion of the electrical powertrain used to emulate the turbofan engine is shown in blue, while the experiment EAP powertrain is shown outlined in red in Fig. 1b.

A. Hybrid Propulsion Emulation Rig

The smaller scale HyPER is an ideal space to demonstrate rapid prototyping for low TRL control technologies leading to faster verification and validation. A block diagram overview of the main components of HyPER is shown in Fig. 2. It includes four permanent magnet synchronous Electric Machines (EM)s coupled together by two shafts to form two EM systems, four inverters, a DC-DC converter, and a supercapacitor bank, all of which represent the scaled electrified turbomachinery. The testbed also contains two bi-directional power supplies, two heat exchangers, and a resistive load bank. One bi-directional DC power supply is used to power the gas turbine emulation electric machines (highlighted in blue). The second bidirectional power supply is used to either emulate energy storage devices or provide an additional electrical load (highlighted in red).

A real-time computer with a graphical user interface commands the system and monitors the recorded data with measurements and components. The main electrical powertrain components are mounted to a table that can be moved in and out of the test cell for staging purposes or replaced with a different electro-mechanical system. Supporting equipment that remains inside the test cell includes the power supplies and break resistor. This functionality facilitates rapid testing of different electrical architectures and associated control. A unique aspect of this testbed is the inclusion of energy storage in the form of a supercapacitor bank. The energy storage device allows for energy management control concepts to be implemented with hardware.

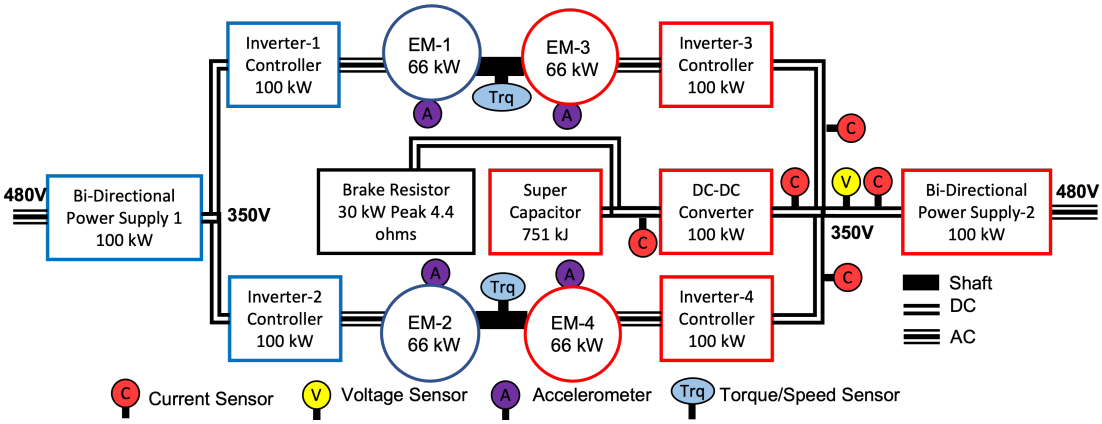

Fig. 2 HyPER facility hardware in the loop block diagram for hybrid turbofan real-time emulation and powertrain.

B. NASA Electric Aircraft Testbed

The NEAT facility is designed as a reconfigurable testbed capable of testing electro-mechanical and EAP systems at relevant power and altitude conditions for single-aisle aircraft. The facility can accept up to 24 MW of electrical power and operate at voltage levels as high as 4500 Volts DC [12]. The altitude capabilities were not required for the controls testing discussed in this paper. An overview of two tests at NEAT are outlined in this paper, the first focused on controls studies at the propulsion system level and the second is focused on controls studies at the aircraft level.

1. NEAT Hybrid Turbofan Testing

In the controls test configuration, NEAT can supply up to 1.5 MW of electrical power at 700 VDC, which is sufficient to emulate the scaled power system. The NEAT facility hardware layout for the tests consists of 8 250 kW permanent magnet synchronous EMs configured on two shafts, 4 machines to a shaft. A diagram illustrating the hardware layout is shown in Fig. 3. Each EM is controlled by a matching inverter controller and operates on 3-phase AC power. On each shaft, two of the EMs are connected to a common DC bus while the remaining two EMs are connected to the opposite DC bus. The experiment bus represents the electro-mechanical hardware integrated into the hybridized turbofan, specifically the Low Pressure Spool (LPS) and High Pressure Spool (HPS) EMs and motor controllers. The emulation bus is used to represent the turbofan engine and emulates the torque response of the engine shafts to the inputs from the experiment side. Each DC bus is powered by three 250 kW unidirectional power supplies, which are used to regulate the

buses to a constant 700 VDC. Each bus is also connected to a reconfigurable load bank, adjustable in steps up to 1 MW. The system can sink up to 2 MW of power in total. It should be noted that NEAT does not currently have the capability for energy storage testing as outlined for the HyPER testing.

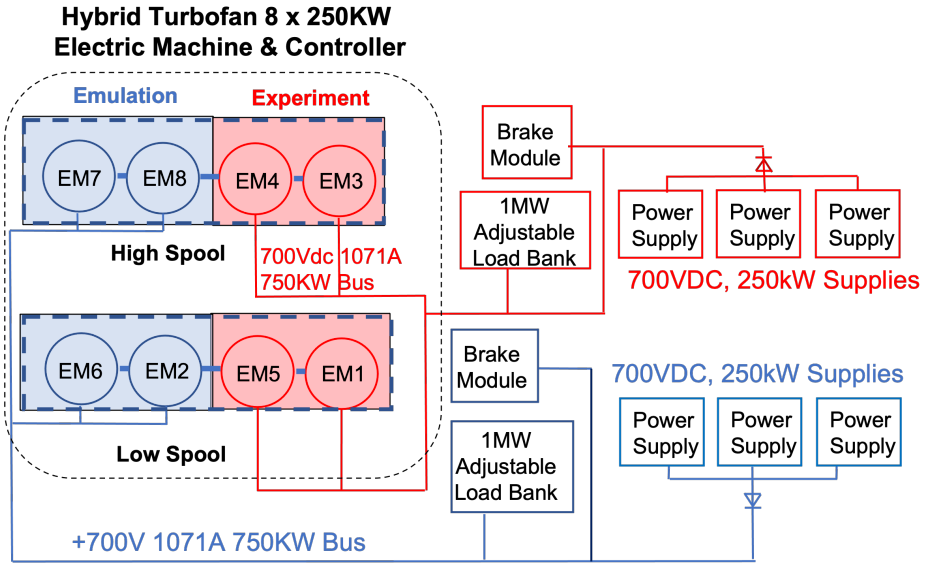

Fig. 3 NEAT facility hardware in the loop block diagram for hybrid turbofan real-time emulation (blue) and electrical powertrain (red). Here the electric machine and controller are referred to as EM, for a total of 8 representing the hybrid turbofan.

2. NEAT Vehicle Propulsion System Level Testing

The NEAT vehicle propulsion system level control study evaluated a control design developed for the propulsion system of the Single-aisle Turboelectric AiRCraft with Aft Boundary Layer propulsor (STARC-ABL) NASA concept aircraft [21]. The STARC-ABL is a turboelectric design that exhibits electromechanical coupling between its subsystems and requires an integrated system-level control strategy to ensure optimal efficiency and operability. The STARC-ABL exhibits the electromechanical coupling between subsystems inherent in many EAP designs making it a good candidate for conducting EAP integrated controls research. A depiction of the STARC-ABL concept and its mechanical-electrical architecture is shown in Fig. 4.

This partially turboelectric concept architecture consists of two wing mounted geared turbofan engines and a motor-driven boundary layer ingesting tailfan propulsor. The geared turbofan engines serve the dual purpose of producing thrust and generating electrical power to drive the tailfan motor. Electric generators connected to the low-pressure shaft of each turbofan are configured to supply power to a direct current (DC) bus to maintain a constant voltage level. Connected to this same DC bus is a 3500-horsepower electric motor used to drive the tailfan. In this configuration the STARC-ABL exhibits an aft-to-forward coupling. Any change in the tailfan motor power demand will result in a corresponding change in the amount of power the generators must extract from the turbofans to hold the bus voltage constant. It is also a multi-input multi-output (MIMO) control design problem in the sense that there are multiple inputs (fuel flow and motor torque) used to control multiple outputs (turbofan and tailfan corrected fan speed) [22].

The NEAT electrical hardware setup for the STARC-ABL is nearly identical to that outlined in Fig. 3. The primary differences being the top string of EMs (3,4,7,8) represents the tail fan, the shaft connection between EM 2 and EM 5 is disconnected to represent the two geared turbofans, and finally EM 2 and EM 5 swap electrical connections to change to the experiment and emulation buses respectively [17].

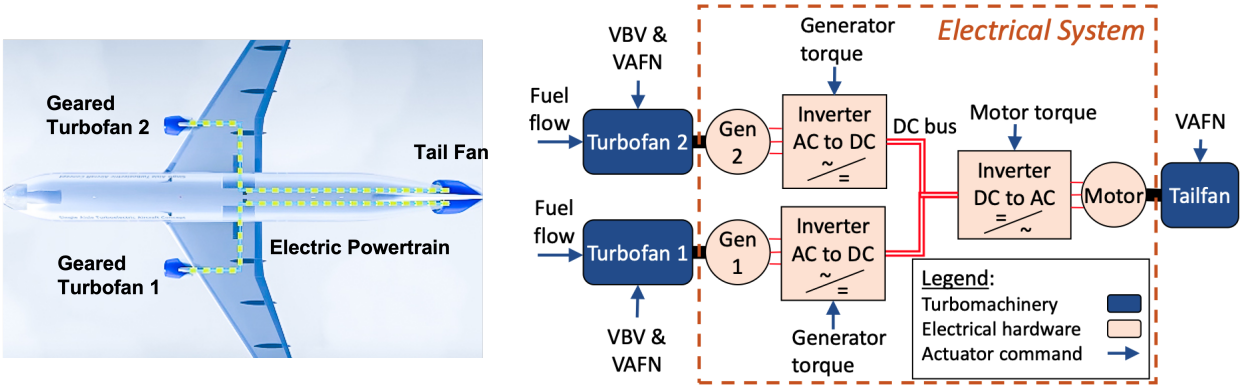

(a) STARC-ABL EAP Concept. **(b) STARC-ABL Architecture.**

Fig. 4 Conceptual STARC-ABL aircraft system (a) is artistic image of aircraft with key features denoted, (b) is a block diagram of the turbomachinery and electrical powertrain components.

III. Modeling and System Scaling

To emulate the propulsion system in a HIL environment, a real-time model of the system is needed. The following subsections will cover the propulsion system model tested at both facilities, the STARC-ABL aircraft level model tested only at NEAT, their respective control systems, the dynamic scaling, and real-time implementation. A modified version of the Advanced Geared Turbofan (AGTF30) engine model is used to facilitate the development of a hybrid-turbofan [23, 24]. The AGTF30 is a conceptual commercial transport turbofan engine that is modeled within MATLAB/Simulink using the Toolbox for Modeling and Analysis of Thermodynamic Systems (T-MATS) [25]. Details of the STARC-ABL modeling approach are in Ref. [17, 26]. All test scenarios at each HIL facility underwent a pre-test simulation analysis using the described models. This enabled evaluation and refinement of the control design to ensure that desired system performance and operability was maintained over all planned test scenarios.

A. Hybrid Turbofan Models and Controls

The AGTF30 is a 30,000 lbf thrust class conceptual advanced gear turbofan engine with technologies suitable for the 2030s timeframe that includes a compact core and variable area fan nozzle[27]. The hybrid AGTF30 features dual spool EMs, power electronics, and energy storage. The turbomachinery is modeled at the component level and maps are used to characterize the performance of compressors and turbines. Shaft dynamics are included by using the imbalance of torques on the shafts to calculate a rate of change in speed. To account for the impact of the EMs on the shaft dynamics the torque summation in the model is modified to include the additional EM torque inputs.

The hybrid AGTF30 electrical system (i.e., LPS EM and HPS EM) and the HIL components are modeled using the PowerFlow blockset of the Electrical Modeling and Thermal Analysis Toolbox (EMTAT) [28]. EMTAT is designed to interface with T-MATS as a complementary set of library blocks. The component based EMTAT model uses simple efficiency tables to predict the voltage, current, and power losses of each component in the power system at a fidelity compatible with the real-time turbomachinery model. Rapid electrical transients were neglected as they occur on timescales far shorter than turbomachinery dynamics. The electrical system high-speed transients (on the nanosecond or microsecond timescale) are smoothed out over a given time step. This does not replace high speed, high fidelity electronic simulation tools such as the Simulation Program with Integrated Circuit Emphasis (SPICE). However, since EMTAT simulates significantly faster than real time, it is useful for testing control concepts [29]. In addition, EMTAT model blocks can simulate heat outputs and thermal rises, with associated performance impacts. The EMTAT model is used prior to test to predict the amount of electrical power required by the EAP HIL system. During HIL controls testing of the augmented hybrid AGTF30, the electrical powertrain is removed from the real-time simulation, and replaced with electrical hardware in the HIL testbeds.

The Turbine Electrified Energy Management (TEEM) control approach is used to modify the baseline fuel flow controller of the hybrid AGTF30 propulsion model. This controls approach provides a means for improving and tightly regulating the operability margin of electrified turbomachinery [24]. A high level overview of the approach is provided here, with a simple block diagram of the hybrid turbofan control architecture is shown in Fig. 5. The pilot sets the

desired power lever angle (PLA) and the AGTF30 TEEM controller then sets the main fuel flow command along with the torque commands. The primary sensed feedback for the turbomachinery is shaft rotational speed and for the power system it is the Energy Storage Device (ESD) state of charge.

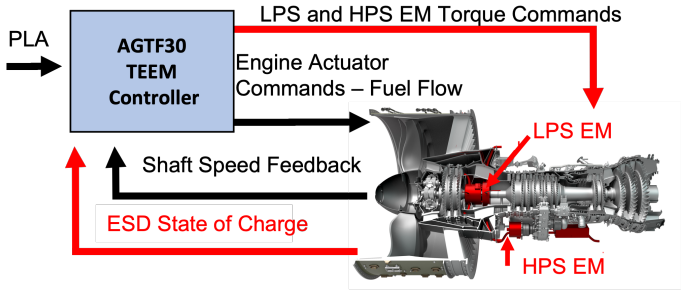

Fig. 5 Block diagram of the hybrid turbofan control architecture, where black indicates traditional turbofan control and red indicates hybrid components.

The control concept takes advantage of EMs and small energy storage devices as new actuators to benefit the operation of the turbofan. A major goal of TEEM is the improvement of transient operability margin. Engine operability, particularly compressor stability margin, often degrades during engine transients (when there is a large rapid change in power level). This degradation in operability margin must be accounted for in the turbofan design and thus places constraints to ensure safe operation, leading to sacrificed performance to guarantee operability margin [30]. The electric powertrain provides a new mechanism to tightly control the turbofan operability margins and expands the design space to potentially achieve better performance. TEEM uses the EMs coupled to the shafts of the engine to maintain the steady state speed vs. fuel flow relationship during transients. This keeps the flow state within the engine in sync with the system inputs. This reduces the mismatch in the shaft speed and flow state that occurs due to shaft dynamics and differences in the low spool and high spool inertias. Beyond the transient operability benefits, TEEM has also been shown to have benefits for modifying nominal operation. For example, power addition to or extraction from the engine shafts can be used to reduce the need for, or even replace, the function of stability bleeds [31–35].

B. Vehicle Propulsion System Model and Control

To model the STARC-ABL concept propulsion system the same general procedure is used as outlined above for the hybrid AGTF30. The turbomachinery models are scaled versions of the AGTF30 for the two wing mounted turbofans, and the tailfan uses a ducted fan modeling block from the T-MATS library. The electrical system uses EMTAT blocks to represent the hardware discussed below. A key aspect of the integrated control design approach is the implementation of a single PLA throttle command from the aircraft, shown in Fig. 6. This is a departure from conventional commercial aircraft vehicle-propulsion interface designs where separate throttle inputs are available to independently control the operation of each engine installed on the vehicle. The single throttle approach is implemented here to guard against uncoordinated operation of the turbofan and tailfan subsystems. In sever cases, uncoordinated subsystem operation can cause turbofan compressor stalls. The solution applied to address this transient mismatch concern is to calculate and supply a "synthesized" PLA command input signal to the tailfan power management schedule. The synthesized PLA command is a function of the average sensed $N1c$ of the two turbofans and equates to the PLA setting that would produce that same $N1c$ under steady-state conditions. Applying the tailfan synthesized PLA promotes more synchronized operation of the turbofan and tailfan subsystems for a coordinated response during both acceleration and deceleration transients.

A summary of the STARC-ABL integrated control design is provided in Ref. [22]. A block diagram of the STARC-ABL and the developed control system is shown in Fig. 6. Each turbofan has a proportional integral (PI) fuel controller that produces a fuel flow command, wf_{cmd}, based on the error between commanded corrected fan speed, $N1c_{cmd}$, and sensed corrected fan speed, $N1c$. The tailfan has a PI motor controller that produces a motor torque command, Q_{cmd}, based on the error between commanded corrected tailfan speed, Ntc_{cmd}, and sensed corrected tailfan speed, Ntc. The commanded speed setpoints for the turbofans and tailfan are provided by the power management schedule blocks shown in the figure. The power management schedules define the target subsystem thrust output based on cockpit throttle position and flight condition. They are implemented as multi-dimensional lookup tables that accept

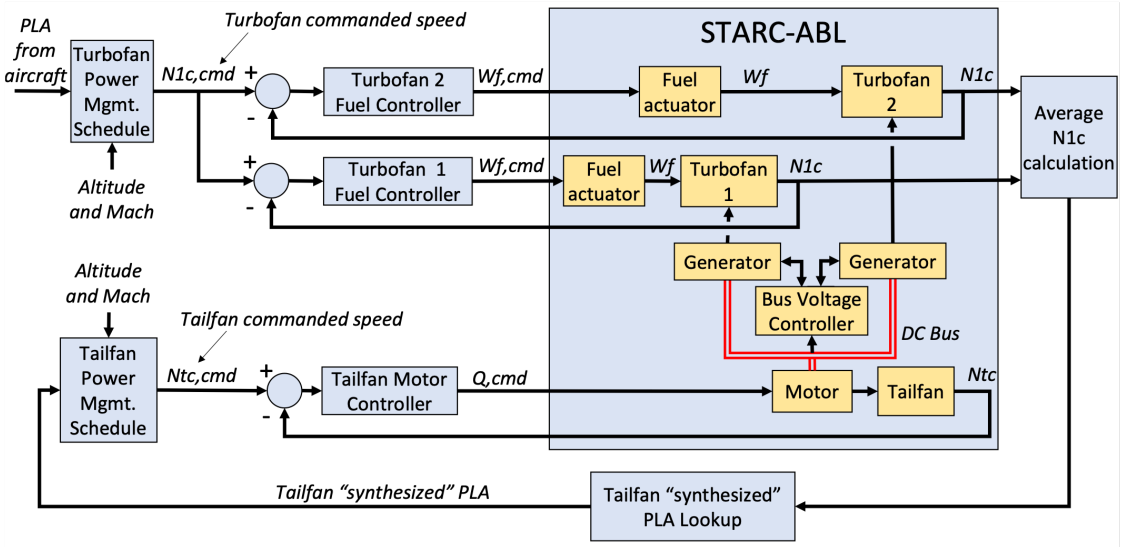

Fig. 6 STARC-ABL closed loop control architecture.

inputs of altitude, Mach number, and throttle position (denoted as PLA) and produce corrected speed setpoint outputs. Under most operating conditions, the schedules result in the generators extracting approximately 28% of the total power delivered to the LPS of each turbofan by its low-pressure turbine. This level of power extraction allows the steady-state operating line of the turbofans to reside near a region of peak efficiency, particularly when operating at cruise conditions. The 28% power extraction level is maintained at all operating conditions where the tailfan motor remains below its maximum 3500hp limit. However, high PLA settings at low to intermediate altitudes will result in the tailfan reaching the 3500hp maximum, resulting in tailfan speed and thrust output limiting. Under such conditions, increasing PLA beyond the point where the motor limit is encountered will cause an increase in turbofan speed and thrust output while the tailfan motor speed and thrust remains "plateaued" at the limit.

C. Sliding Mode Impedance Controller with Scaling

A key enabling component of the controls HIL testing performed at HyPER and NEAT is a dynamic scaling and emulation controller that enables the torque response of the turbomachinery shafts to be emulated using the smaller electrical hardware. When using EMs to emulate turbomachinery, they differ in three main categories: power, angular inertia, and angular viscous friction [36, 37]. The solution to the power discrepancy is to scale any full-scale commands or sub-scale feedback signals passed between the full-scale model and the sub-scale system as shown in Fig. 7. Scaling commands to and from the systems ensures that the sub-scale system operates within its capability range when being controlled by a full-scale model. Discrepancies in the angular inertia and viscous friction cause differences in the hardware shaft speed response when provided identical torque inputs from the shaft software model. A solution is to use closed loop control to modify the dynamic response characteristics of the sub-scale hardware system so that its behavior is a sub-scale representation of the full-scale software model.

The developed Sliding Mode Impedance Controller with Scaling (SMICS) is applied to cause the EMs on the emulation bus (blue) to mimic the scaled inertial load of the turbofan shaft when subjected to the torques applied by the experiment hardware (red) [36, 37]. Closed-loop control is implemented over the commanded shaft speeds, with torque, inertia, and power scaling that adjusts the engine torques and speeds to levels that can be achieved by the HyPER or NEAT EMs. Application of the SMICS algorithm allowed the full-scale electrified propulsion control design discussed in this paper to undergo testing at HyPER and NEAT without modification or the inclusion of physical gas turbine hardware. A diagram of the engine model and closed-loop hardware control with SMICS is shown for one shaft in Fig. 7 and the algorithm derivations is provided in Ref. [37].

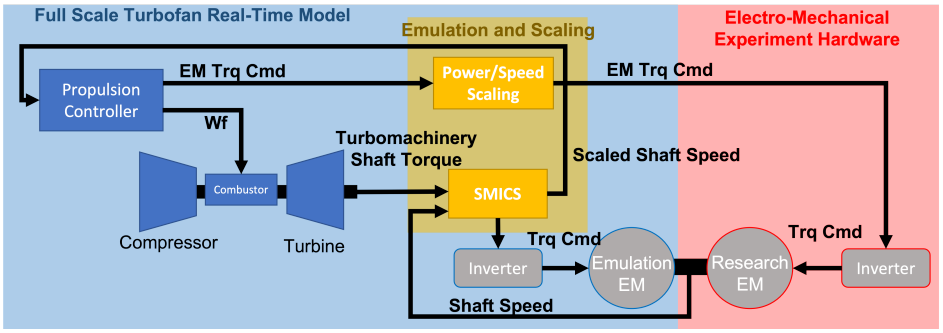

Fig. 7 Sliding mode impedance controller for scaling of a single shaft of the turbofan emulation (blue) with experiment bus hardware (red).

D. Real-Time Model Implementation

For each HIL test, the propulsion system and the control design software are coded as a real-time application and implemented in a dSPACE SCALEXIO real-time computing system. For the real-time model the electrical model is replaced with the physical hardware. The real-time application, which directs the operation of the electric motors, is employed to meet the strict time constraints required by the hardware in-the-loop control test. This application is built using dSPACE ConfigurationDesk, which compiles the MATLAB and Simulink code related to the engine model, controller, and the command and data handling system. A graphical user interface, developed using dSPACE ControlDesk, allows the operator to send commands to the application, edit test-specific settings, check the status of faults and alarms, view telemetry from the test hardware, and display data from Simulink models processed in real-time.

IV. Results

The results that follow give an overview of the EAP controls HIL tests. Testing the controllers with hardware-in-the-loop involved running the real-time models through various throttle profiles at different simulated altitude and Mach number conditions throughout the flight envelope. In addition, example mission profiles are used to evaluate the controllers under typical flight conditions. A representative selection of the full test results is provided, starting with the electrical system modeling, to demonstrate pre-test prediction fidelity of the electrical components using EMTAT. Results are then provided for the aircraft level testing conducted at NEAT for the STARC-ABL concept. Finally, results are provided at the propulsion system level at both the HyPER and NEAT facilities.

A. Electrical Model Results

After HyPER was configured, a series of "characterization" runs were performed to assess the operational characteristics of the rig over a range of speeds and torques spanning the EM's operating envelope. During each characterization run, one EM was commanded to hold a constant shaft speed while the companion EM connected to the same shaft applied varying levels of commanded torque insertion or extraction. Test data acquired from these characterization runs is used to validate the accuracy of the EMTAT library blocks applied to model the HyPER electrical system. Table 1 lists example results comparing steady-state EMTAT simulation outputs against HyPER laboratory averaged and filtered data acquired during a 2000 RPM characterization run conducted on the shaft comprised of motor 2 (M2) and motor 4 (M4). Nearly all the key model parameters matched the HyPER test results within 1% and the model was found to transition smoothy from positive to negative power on any given device. Across the entire characterization test series, beyond those shown here, only one key model parameter differed by more than 5% and nearly 70% were within 1% [29].

B. STARC-ABL Aircraft System Results

The test matrix for the NEAT STARC-ABL controls test consists of the following test card types: throttle profile test cards, mission profile test cards, and simulated abrupt fault test cards [17]. For this paper example results are shown for a mission profile test card that subjects the STARC-ABL control design to altitude, Mach, and PLA variations for a

Table 1 Comparison of predicted EMTAT data and HyPER test averaged data using percent difference during facility characterization testing at 2,000 rpm [29].

Command Torque	M2 Speed	M2 DC Bus Current	M2 Torque Feedback	M4 Speed	M4 DC Bus Current	M4 Torque Feedback
-130 Nm	0.1 %	-0.7 %	0.4 %	0.1 %	2.7 %	0.0 %
-50 Nm	-0.1 %	-0.5 %	-0.1 %	0.0 %	1.0 %	0.0 %
-10 Nm	0.0 %	0.3 %	0.2 %	0.0 %	0.4 %	0.0 %
10 Nm	0.0 %	0.3 %	0.2 %	-0.1 %	0.2 %	0.0 %
50 Nm	0.0 %	0.6 %	0.7 %	0.0 %	0.9 %	0.0 %
130 Nm	0.1 %	-3.41 %	-0.1 %	0.1 %	1.6 %	-0.2 %

full-flight profile. The mission profile is shown in Fig.8 and is based on actual data from a 70-minute flight acquired from the NASA Ames Research Center DASHLink [38]. Highlighted in light grey is the takeoff portion of the mission profile and the decent is highlighted in dark grey.

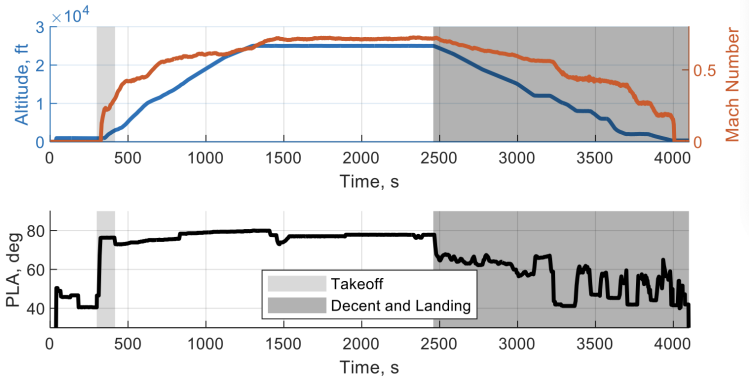

Fig. 8 Flight mission profile using flight data from DASHLink.

The STARC-ABL NEAT Mission profile full-scale results for the flight data mission are shown in Fig. 9. Given that the STARC-ABL's two geared turbofans operate symmetrically, results from only one turbofan are provided. Parameters shown include full-scale rotational speeds, stall margins, tailfan motor torque, and turbofan generator torque. Each figure shows actual full-scale experimental results obtained during NEAT testing (blue lines) compared against pre-test simulation predictions (dashed red lines). The NEAT generator and motor torque data shown in the figure are direct scaled representations of the torque applied to the NEAT EMs. The tailfan and turbofan LP speeds shown in the figure are filtered values obtained via a low pass filter, but are otherwise also a direct scaled representation of the NEAT hardware rotational speeds. The flight data profile, based on actual aircraft flight data, exhibits variability in PLA, particularly during the descent phase of the flight profile. Good agreement between the experimental results and pre-test simulation predictions are observed in all mission phases. In all test cases the STARC-ABL system controller performed as intended. These results are encouraging as they further demonstrate the robust performance of the control design when subjected to realistic variations in flight condition and PLA movements.

C. AGTF30 Propulsion System Results

The results for the propulsion system will first highlight a unique feature of the HyPER facility and then focus on a comparison of results between HyPER and NEAT. A key feature of the HyPER lab is the inclusion of a physical energy storage device in the form of a supercapacitor bank and associated DC-DC converter. Accurately predicting the energy state of the supercapacitor bank is essential to ensuring the operation remains within its capability limits. In general,

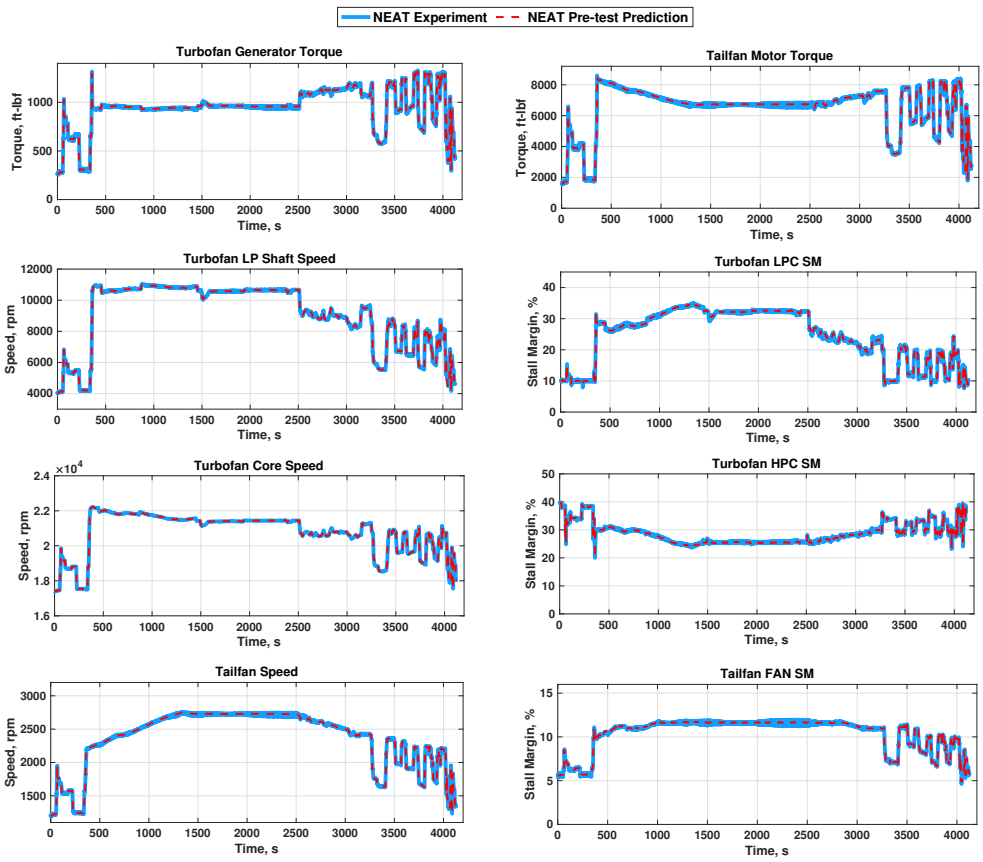

Fig. 9 STARC-ABL NEAT results for the flight mission profile [17].

the supercapacitor bank voltage is predicted within a small error. This is illustrated using the takeoff profile shown in Fig. 10. Pre-test model electrical parameter predictions provide a sufficient degree of agreement, as shown for the supercapacitor bank voltage, supercapacitor bank current, and DC-DC converter bus-side current measurement during the profile. For the comparisons with NEAT experimental results that follow, the real-time model assumes perfect knowledge of the required energy storage device state of charge required for the TEEM controller.

The following results demonstrate performance of a scaled hybrid propulsion system model (AGTF30) with a TEEM controller, verifying that inclusion of the physical electrical power system and associated constraints do not significantly diminish capability. These constraints include factors such as torque ramp rate limits, sensor bias and noise, and inverter controller tuning that impact the controller and its effectiveness. The PLA throttle profile applied for a sea level static (altitude = 0 ft, Mach number = 0) test card with multiple throttle movements and a more aggressive snap burst/chop throttle movement is shown in Fig. 11. This test card is used as a representative example from the extensive testing conducted. Both HyPER and NEAT data is presented to illustrate the effects of scaling between the two facilities.

Pre-test predictions are shown in Table 2 and compared to experimental results for the electric machines that represent both the experimental components and emulation of each shaft of the turbofan for speed and power. The example test card is selected to demonstrate the TEEM control models across a range of power levels including the most aggressive PLA movements. The relative error is calculated as a root-mean-square relative error (RMSRE) between the pre-test prediction and the measured experimental results. The RMSRE for each measurement is normalized by the magnitude of the maximum predicted value of that parameter. The different noise signatures between the pre-test simulation and measured experimental results are handled by smoothing the data with a locally weighted regression [20]. For the EM power calculations, the DC voltage and current measured at the inverter inputs were multiplied to get

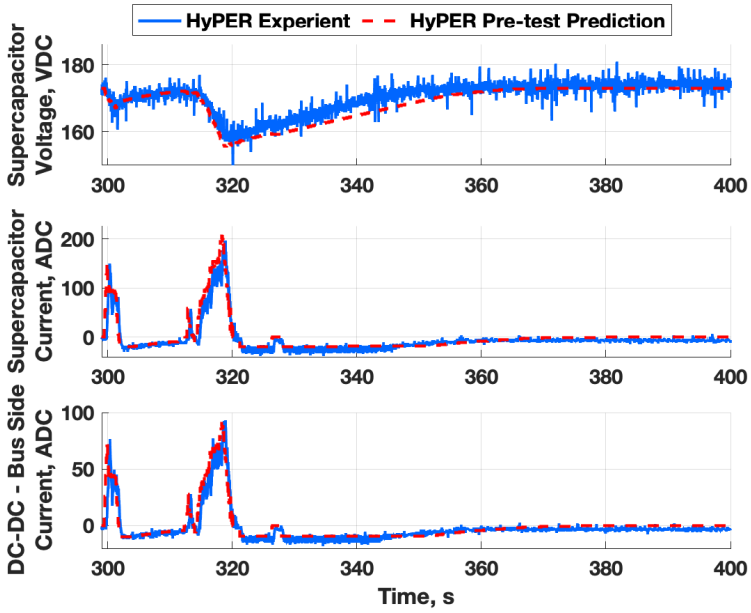

Fig. 10 HyPER supercapacitor and DC-DC converter electrical signals during mission profile takeoff [18].

the electrical power. For the NEAT configuration where two EMs are used for each side of the turbofan's LPS and HPS, the total power for each pair of EMs is determined by calculating the power of each individual EM, and then summing the results.

Table 2 Comparison of predicted and experimental parameters between NEAT and HyPER using normalized RMSRE during the sea level static example test card.

Facility	Scaled LPS Speed	Scaled HPS Speed	LPS Experiment EM Power	HPS Experiment EM Power	LPS Emulation EM Power	HPS Emulation EM Power
HyPER	0.4%	0.2%	4.0%	2.7%	5.5%	3.2%
NEAT	0.1%	0.1%	2.3%	3.1%	3.3%	3.7%

Table 2 lists the RMSRE of key parameters at both the NEAT and HyPER facility. The comparison between predicted and experimental results are in close agreement and does not exceed 6% for the measured EM electrical power and remains below 0.5% for the shaft speeds. At both the NEAT and HyPER facility it is found that the largest error is for the EM power on the LPS. A key finding is that the error is similar in value when comparing between the NEAT facility with larger EMs and HyPER with smaller EMs. This finding illustrates that the sliding mode impedance controller, shown in Fig. 7, is able to provide accurate emulation of physical hardware dynamics at the larger or smaller scale facilities. Given the cost and schedule pressure at larger facilities, the ability to conduct feasibility control studies at small scale facilities such as HyPER with greater confidence in the results is important for future work.

The sea level static example test card is also used to compare the full-scale model pre-test predictions and the real-time model implemented with experimental results being used as the feedback. Typical engine sensed parameters are shown in Fig. 12. The parameters include LPS rotational speed, $N2$, HPS rotational speed, $N3$, engine exhaust gas temperature, $T45$, compressor exit pressure, $Pt3$, fuel flow rate, Wf, High Pressure Compressor, (HPC), Stall Margin (SM), Low Pressure Compressor (LPC) SM and net thrust, $Fnet$. The AGTF30 controller sets the Wf to achieve a desired $Fnet$ while maintaining SM stability objectives using the defined sensed parameters. The transient results of the key engine parameters illustrate close agreement between each facility's pre-test predictions ("Pre") and experimental results ("Exp") shown in Fig. 12. In addition, the comparison between the NEAT and HyPER facilities demonstrates a close agreement in time, even during larger transients. HyPER transient responses of the LPC SM have

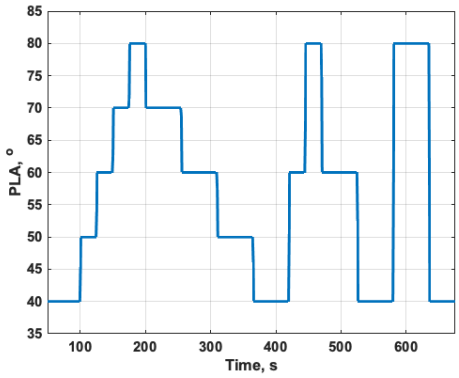

Fig. 11 Sea level static example test card for PLA input variation using AGTF30 with the TEEM controller.

the largest deviations from predicted values at 300s and 400s, where the experimental results have better performance than predicted. The close comparison is, in part, the result of the primary experimental hardware feedback to the real-time model being rotational shaft speed, which generally has little measurement error. The combination of the results listed in Table 2 and shown in Fig. 12 provides confidence in the value of testing control algorithms at the smaller scale facilities to gain insights ahead of testing with development hardware at full-scale facilities.

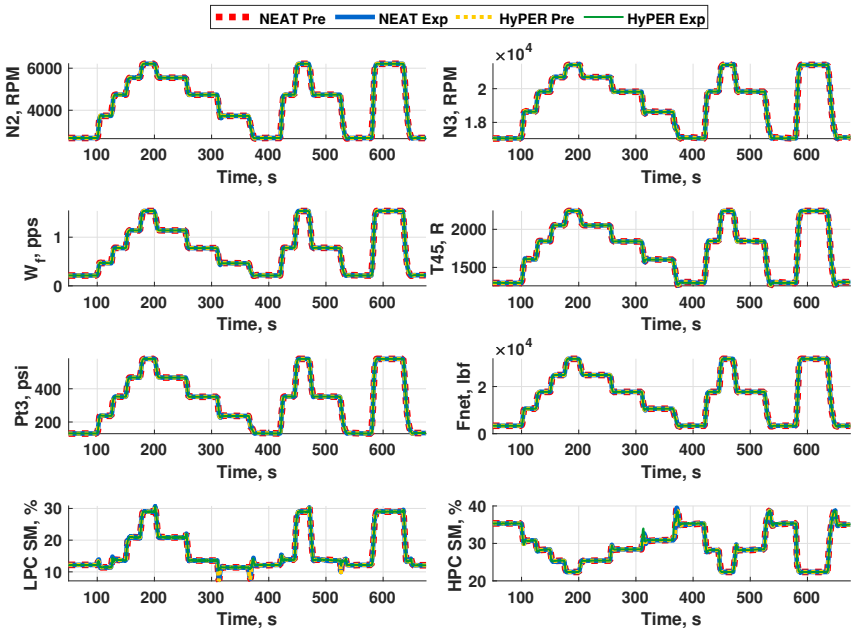

Fig. 12 Comparison of HyPER and NEAT engine model parameters during a sea level static example test card, where "Pre" refers to the pre-test prediction and "Exp" refers to experimental results.

V. Conclusions

Electrified Aircraft Propulsion (EAP) systems hold potential for the reduction of aircraft fuel burn and emissions. To fully realize this potential, the maturation of control technology will be critical. This includes Hardware-In-the-Loop (HIL) studies of control designs that facilitate the coordinated operation of the tightly coupled electrical powertrain and

turbomachinery that comprise EAP systems. Reconfigurable HIL testbeds enable the study of integrated supervisory control and control approaches that augment engine shaft torques to improve performance. This paper presented an overview of EAP controls testing of conceptual designs in two HIL testbeds. The NASA Electric Aircraft Testbed (NEAT) provides the ability for megawatt class electric powertrain testing for technology maturation. A 100 kilowatt testbed, the Hybrid Propulsion Emulation Rig (HyPER), allows for rapid controls technology trade studies. For both testbeds the electrical power system is implemented in hardware, turbomachinery is emulated via electric machines that are commanded by a real-time model and controls. A novel scaling algorithm is applied to emulate the inertial loads of the turbomachinery that causes the electric machines to respond similarly to the full-scale propulsion system they represent. A comparison between predicted and experimental results was provided for a flight mission profile and sea level static burst/chop test card that demonstrated close agreement. In addition, comparisons of results between HyPER and NEAT showed similar errors at each facility and similar trends. This finding illustrates that the sliding mode impedance controller can emulate the hardware dynamics. Gaining confidence in controls studies from smaller scale facilities such as HyPER is important to future work since the cost and schedule pressure at larger facilities does not lend to them to be readily available.

Acknowledgment

The authors would like to thank the Hybrid Thermally Efficient Core project, Advanced Air Transport Technology project, and the Transformational, Tools, and Technology project under the NASA Aeronautics Mission Directorate for their support of this work. None of this work would have been possible without the technician team and subject matter experts support in the design and buildup of the Hybrid Propulsion Emulation Rig or the test support team at the NASA Electric Aircraft Testbed.

References

[1] Nolen, B., "2021 Aviation Climate Action Plan," FAA Report, 2021.

[2] Pearce, R., "NASA Aeronautics Strategic Implementation Plan," NASA NP 2017-01-2352-HQ, 2019.

[3] Grewe, V., Gangoli Rao, A., Grönstedt, T., Xisto, C., Linke, F., Melkert, J., Middel, J., Ohlenforst, B., Blakey, S., Christie, S., Matthes, S., and Dahlmann, K., "Evaluating the climate impact of aviation emission scenarios towards the Paris agreement including COVID-19 effects," *Nature Communications*, Vol. 12, No. 1, 2021, pp. 1–10. https://doi.org/10.1038/s41467-021-24091-y.

[4] Jain, S., and Crossley, W. A., "Predicting fleet-level carbon emission reductions from future single-aisle hybrid electric aircraft," AIAA 2020-3554, 2020. https://doi.org/10.2514/6.2020-3554.

[5] Simon, D. L., Connolly, J. W., and Culley, D. E., "Control Technology Needs for Electrified Aircraft Propulsion Systems," *Journal of Engineering for Gas Turbines and Power*, Vol. 142, No. 1, 2020, pp. 1–10. https://doi.org/10.1115/1.4044969.

[6] Miller, C., Zumberge, J., Corbett, M., Wolff, M., and Russell, G., "Low Spool Electrical Power Extraction Using Hardware-in-the-Loop Methods," AIAA 2010-7091, 2010. https://doi.org/10.2514/6.2010-7091.

[7] Himmler, A., "Openness requirements for next generation hardware-in-the-loop testing systems," AIAA 2014-0636, 2014. https://doi.org/10.2514/6.2014-0636.

[8] Nawash, N. S., Sadey, D. J., and Howard, R., "Power Quality Analysis for a High Voltage Power System for Urban Air Mobility Application," AIAA 2021-3308, 2021. https://doi.org/10.2514/6.2021-3308.

[9] Sadey, D. J., Bodson, M., Csank, J. T., Hunker, K. R., Theman, C. J., and Taylor, L. M., "Control demonstration of multiple doubly-fed induction motors for hybrid electric propulsion," NASA/TM 2020-220384, 2020. https://doi.org/10.2514/6.2017-4954.

[10] Bodson, M., Sadey, D. J., Hunker, K. R., Theman, C. J., Taylor, L. M., and Csank, J. T., "Hybrid electric propulsion using doubly fed induction machines," *Journal of Propulsion and Power*, Vol. 36, No. 1, 2020, pp. 78–87. https://doi.org/10.2514/1.B37415.

[11] Enalou, H. B., Rashed, M., Kulsangcharoen, P., Chowdhury, S., and Bozhko, S., "A Twin Spool Engine Emulator for the Study of Power Exchange Idea," ITEC 2018-8607540, 2018. https://doi.org/10.1109/ESARS-ITEC.2018.8607540.

[12] Haglage, J. M., and Brown, T. W., "Nasa electric aircraft testbed (Neat) reconfiguration to enable altitude testing of megawatt-scale electric machines," *AIAA Propulsion and Energy 2020 Forum*, 2020, pp. 1–13. https://doi.org/10.2514/6.2020-3561.

[13] Choe, J. M., Channegowda, P., and Wu, X., "Development of High Bandwidth Power Hardware-in-Loop Test Platform for Aircraft Hybrid Electric Propulsion," AIAA 2021-3325, 2021. https://doi.org/10.2514/6.2021-3325.

[14] Choi, B. B., and Brown, G. V., "Propulsion powertrain real-time simulation using hardware-inthe-loop (HIL) for aircraft electric propulsion system," AIAA 2017-4703, 2017. https://doi.org/10.2514/6.2017-4703.

[15] Khamvilai, T., Pakmehr, M., Lu, G., Yang, Y., Feron, E., and Behbahani, A., "Hardware-in-the-Loop Simulation Testbed Development for Distributed Turbine Engine Control Systems," AIAA 2022-1233, 2022. https://doi.org/10.2514/6.2022-1233.

[16] Thomas, G. L., Culley, D. E., and Brand, A., "The application of hardware in the loop testing for distributed engine control," AIAA 2016-4654, 2016. https://doi.org/10.2514/6.2016-4654.

[17] Simon, D. L., Bianco, S. J., and Horning, M. A., "Real-time Hardware-in-the-Loop Evaluation of a Partially Turboelectric Propulsion Control Design," AIAA To Be Published, 2023.

[18] Bianco, S. J., Kratz, J. L., Culley, D., and Horning, M., "Hybrid-Electric Aero-Propulsion Controls Testbed Results with Energy Storage," AIAA To Be Published, 2023.

[19] Buescher, H., Culley, D., Bianco, S., Connolly, J., Dimston, A., Saus, J., Theman, C., Horning, M., Hunker, K. R., Garrett, M. J., Haglage, J. M., and Cha, Y. C., "Hybrid-Electric Aero-Propulsion Controls Testbed : Overview and Capability," AIAA 2023-0671, 2023. https://doi.org/10.2514/6.2023-0671.

[20] Sachs-wetstone, J. J., Bianco, S. J., Kratz, J. L., and Horning, M., "Hybrid-Electric Aero-Propulsion Controls Testbed Results," AIAA To Be Published, 2023.

[21] Welstead, J., and Felder, J. L., "Conceptual Design of a Single-Aisle Turboelectric Commercial Transport with Fuselage Boundary Layer Ingestion," *54th AIAA Aerospace Sciences Meeting*, AIAA-2016-1027, 2016, pp. 1–17. https://doi.org/10.2514/6.2016-1027.

[22] Simon, D. L., Bianco, S. J., and Horning, M. A., "Integrated Control Design for a Partially Turboelectric Aircraft Propulsion System," ASME-GT2023-100921, 2023.

[23] Chapman, J. W., and Litt, J. S., "Control design for an advanced geared turbofan engine," AIAA 2017-4820, 2017. https://doi.org/10.2514/6.2017-4820.

[24] Kratz, J. L., Culley, D. E., and Thomas, G. L., "A Control Strategy for Turbine Electrified Energy Management," AIAA 2019-4499, 2019. https://doi.org/10.2514/6.2019-4499.

[25] Chapman, J. W., Lavelle, T. M., May, R. D., Litt, J. S., and Guo, T.-h., "Toolbox for the Modeling and Analysis of Thermodynamic Systems (T-MATS) User's Guide," NASA TM 2014-216638, 2014. https://doi.org/10.2514/6.2014-3932.

[26] Kratz, J. L., and Simon, D., "Failure Modes and Mitigation Strategies for a Turboelectric Aircraft Concept with Turbine Electrified Energy Management," AIAA 2022-1191, 2022. https://doi.org/10.2514/6.2022-1191.

[27] Jones, S. M., Haller, W. J., and Tong, M. T., "An N+3 Technology Level Reference Propulsion System," NASA TM 2017-219501, 2017.

[28] Bell, M. E., and Litt, J. S., "Electrical Modeling and Thermal Analysis Toolbox (EMTAT) User's Guide," NASA TM-2020-5008125, 2020.

[29] Bell, M. E., Bianco, S. J., and Litt, J. S., "Comparison of the Electrical Modeling and Thermal Analysis Toolbox Physics Based Model Blocks to Electrified Aircraft Propulsion Motor Test Hardware," AIAA 2023 To Be Published, 2023.

[30] Spang, H., and Brown, H., "Control of Jet Engines," *Control Engineering Practice*, Vol. 7, No. 9, 1999, pp. 1043–1059. https://doi.org/10.1016/S0967-0661(99)00078-7.

[31] Balaghi Enalou, H., and Bozhko, S., "Performance Improvement of Turbofans by Electric Power Transfer," *Journal of Turbomachinery*, Vol. 142, No. 11, 2020. https://doi.org/10.1115/1.4047892.

[32] Kratz, J. L., Culley, D. E., and Lehan, J., "Transient Optimization for the Betterment of Turbine Electrified Energy Management," AIAA 2023-0704, 2023. https://doi.org/10.2514/6.2023-0704.

[33] Chapman, J. W., "Utilizing Electrical Power Extraction for Stability Bleed Reduction within Gas Turbine Engines," AIAA 2021-3477, 2021. https://doi.org/10.2514/6.2021-3477.

[34] Chapman, J. W., "Considering Turbofan Operability in Hybrid Electric Aircraft Propulsion System Design," AIAA 2023-2178, 2023. https://doi.org/10.2514/6.2023-2178.

[35] Kratz, J. L., and Culley, D. E., "Enhancement of a Conceptual Hybrid Electric Tilt-Wing Propulsion System through Application of the Turbine Electrified Energy Management Concept," AIAA 2021-0875, 2021. https://doi.org/10.2514/6.2021-0875.

[36] Bianco, S. J., "Sliding mode transient scaling controller for gas turbine engine emulation on an electric machine," *AIAA Propulsion and Energy 2020 Forum*, 2020, pp. 1–9. https://doi.org/10.2514/6.2020-3677.

[37] Bianco, S. J., and Simon, D. L., "Control and Scaling Approach for the Emulation of Sub-scale Dynamic Mechanical Loads," AIAA 2023 To Be Published, 2023.

[38] Matthews, B., and Oza, N., "Sample Flight Data," , 2012. URL https://c3.ndc.nasa.gov/dashlink/projects/85/.